Am J Physiol Cell Physiol 289: C1220–C1228, 2005.
First published June 15, 2005; doi:10.1152/ajpcell.00164.2005.

Temporal changes of multiple redox couples from proliferation to growth arrest in IEC-6 intestinal epithelial cells

Matias S. Attene-Ramos,[1] Kajorn Kitiphongspattana,[3] Katrin Ishii-Schrade,[1] and H. Rex Gaskins[1,2,3,4]

Departments of [1]Animal Sciences and [2]Veterinary Pathobiology, [3]Division of Nutritional Sciences, and [4]Institute for Genomic Biology, University of Illinois, Urbana, Illinois

Submitted 7 April 2005; accepted in final form 12 June 2005

Attene-Ramos, Matias S., Kajorn Kitiphongspattana, Katrin Ishii-Schrade, and H. Rex Gaskins. Temporal changes of multiple redox couples from proliferation to growth arrest in IEC-6 intestinal epithelial cells. *Am J Physiol Cell Physiol* 289: C1220–C1228, 2005. First published June 15, 2005; doi:10.1152/ajpcell.00164.2005.—Changes in intracellular redox couples and redox reactive molecules have been implicated in the regulation of a variety of cellular processes, including cell proliferation and growth arrest by contact inhibition. However, the magnitude, direction, and temporal relationship of redox changes to cellular responses are incompletely defined. The present work sought to characterize redox and metabolic changes associated with proliferative stages to contact inhibition of growth in rat IEC-6 intestinal epithelial cells. From the first day of culture until 1 day before confluence, an increase in GSH concentrations and a significant reduction in the redox potential of the GSSG/2GSH couple were observed. These changes were accompanied by a decrease in relative reactive oxygen species (ROS) and nitric oxide (NO) concentrations and oxidation of the redox potential of the $NADP^+$/reduced NADP and NAD^+/NADH couples. Postconfluent cells exhibited a significant decrease in GSH concentrations and a significant oxidation of the GSSG/2GSH couple. When cell proliferation decreased, relative ROS concentrations increased ($P < 0.01$), whereas NO concentrations remained unchanged, and the NAD^+/NADH couple became more reduced. Together, these data indicate that the redox potential of distinct couples varies differentially in both magnitude and direction during successive stages of IEC-6 growth. This finding points out the difficulty of defining intracellular redox status at particular stages of cell growth by examining only one redox species. In addition, the data provide a numerical framework for future research of regulatory mechanisms governed by distinct intracellular redox couples.

cell proliferation; contact inhibition; glutathione

CELLS OBTAIN ENERGY from the oxidation of reduced molecules generating a movement of electrons to oxygen or other electron acceptors through several intracellular redox couples (50). Redox mechanisms trigger signaling cascades (35, 55) and modulate cellular processes such as DNA, RNA, and protein synthesis, enzyme activation, and regulation of the cell cycle (1, 11, 12, 21, 26, 43, 54). Special attention has been given to the redox events that trigger or accompany cell proliferation and contact inhibition (5, 18, 22, 42, 53).

Increased concentrations of the tripeptide GSH or reduction of the redox state of the GSSG/2GSH couple measured as an increase in the GSH-to-GSSG ratio or a decrease in the calculated reduction potential derived from the Nernst equation have been associated with cell proliferation (4, 11, 25, 50, 51). A parallel decrease in reactive oxygen species (ROS) production has also been associated with cell proliferation (31, 53). Furthermore, a decrease in the GSH concentration ([GSH])-to-GSSG concentration ([GSSG]) ratio, and the consequent increase in the reduction potential, as well as an increase in ROS production have been associated with decreased cell growth (10, 42, 50, 53).

Conversely, a mitogenic effect of ROS has been proposed (9). Several studies have shown that high ROS concentrations are needed for proliferation (33, 48). In fact, a decrease in ROS and an increase in intracellular low-molecular-weight thiols accompany contact inhibition of cell growth (38, 46). NO-mediated signaling is also involved in both induction (14, 59) and inhibition (2, 16) of cell proliferation as well as the induction of genotoxicity, mitochondrial damage, and apoptosis (30). These differential effects seem to be concentration dependent (13).

The NAD^+/NADH and $NADP^+$/NADPH couples have received less attention regarding their role in cell proliferation (7, 36). NAD works as a carrier, taking electrons from catabolic reactions and redirecting them into the oxidative phosphorylation chain, enabling cells to maximize energy production from catabolic metabolism (34). The NAD^+ concentration ([NAD^+])-to-NADH concentration ([NADH]) ratio plays an important role in regulating intracellular redox and is often considered a readout of the metabolic state (32). Structurally related reduced NADPH is a major source of electrons for reductive biosynthesis and is also used as an electron donor to maintain the overall reduced thiol state in the cell (50). In recent years, there has been increasing recognition that both [NAD^+]-to-[NADH] and [NADPH]-to-[$NADP^+$] ratios and concentrations fluctuate with the physiological state of the cell and affect the ability of certain transcription factors to bind DNA (49, 58).

Overall, there is an apparent contradiction concerning the magnitude and direction of the redox changes experienced by the cell during proliferation and contact inhibition of growth. Depending on how the redox state of the cell is defined (i.e., which redox active species or couple is quantified) and on when it is measured, proliferating cells may appear more reduced or oxidized. The aim of this study was to measure redox and metabolic changes associated with proliferative stages through contact inhibition of growth by using nontransformed intestinal epithelial cells as a model system. The redox state of the GSSG/2GSH and $NAD(P)^+$/NAD(P)H couples, relative concentrations of ROS and NO, and the ATP concentration ([ATP])-to-ADP concentration ([ADP]) ratio were mea-

Address for reprint requests and other correspondence: H. R. Gaskins, Univ. of Illinois, 1207 W. Gregory Drive, Urbana, IL 61801 (e-mail: hgaskins@uiuc.edu).

The costs of publication of this article were defrayed in part by the payment of page charges. The article must therefore be hereby marked "*advertisement*" in accordance with 18 U.S.C. Section 1734 solely to indicate this fact.

sured to establish the magnitude and the temporal relationship of the oxidative and reductive events in an attempt to clarify the previously cited contradictions.

MATERIALS AND METHODS

Reagents. Dispensable amino acids, streptomycin, penicillin, FBS, Trypan blue, trypsin, HBSS, and PBS were purchased from GIBCO (Grand Island, NY). Sodium bicarbonate, HEPES, Hoechst 33342, sulfosalicylic acid (SSA), DTT, *N*-ethylmaleimide (NEM), *ortho*-phthalaldehyde (OPA), GSH, tetrabutylammonium hydroxide, NADH, NADPH, NAD^+, $NADP^+$, ATP, ADP, and propidium iodide were obtained from Sigma (St. Louis, MO). Chloroform, KH_2PO_4, methanol, and sodium bicarbonate were obtained from Fisher (Fair Lawn, NJ). Fungizone was obtained from BioWhittaker (Walkersville, MD).

Cell culture and treatment. The rat intestinal crypt cell line IEC-6 (47) was obtained from the American Type Culture Collection (Manassas, VA), and maintained in DMEM supplemented with glucose (25 mM), and dispensable amino acids (each 0.1 mM), sodium bicarbonate (44 mM), penicillin (40,000 U/l) and streptomycin (40,000 μg/l), HEPES (15 mM), 10% FBS, Fungizone (250 μg/ml), and insulin (0.1 U/ml). Cells were incubated at 37°C in a humidified atmosphere of 5% CO_2 and serially passaged in 75-cm^2 tissue culture flasks (Corning, Corning, NY). Cells were seeded at a density of 1.5×10^5 cells in six-well cell culture plates (area 9.5 cm^2; Corning) and grown for the periods indicated for each experiment. For all experiments, cells were used between *passages 17* and *27*, and cell medium was replaced every 3 days.

Growth curve. IEC-6 cells were seeded at a density of 1.5×10^5 cells per well (6-well plate), cultured, and harvested every day for up to 12 days. After harvesting, the cells were stained with Trypan blue, and live cells were counted with a hemocytometer.

Cell cycle analysis. Cells were seeded in a six-well plate as described above. Each day, cells were washed twice (first with PBS and then with trypsin) and then lifted with trypsin and mixed with 10% FBS in PBS. The cells were centrifuged, fixed with ice-cold ethanol (70%), and kept at −20°C for subsequent analysis. Before the analysis, cells were washed twice in PBS and treated for 30 min with propidium iodide (50 μg/ml) and RNase (100 μg/ml; Qiagen, Valencia, CA). Flow cytometric analysis was performed with an EPICS XL-MCL flow cytometer controlled by SYSTEM II software (Beckman Coulter, Miami, FL). The data were analyzed with Summit V3.1 software (Cytomation, Fort Collins, CO).

Cell volume. Cell volume was estimated with a Beckman Coulter counter (Beckman). A cell volume distribution was performed. A mean cell volume of 1.413 pl (SD 0.507), calculated for early confluent cells, was used to calculate metabolite concentrations.

Cellular DNA quantification. Total DNA concentrations from crude cell homogenates were determined by fluorometry with bisbenzimidazole (Hoechst 33258; Molecular Probes, Eugene, OR) as described previously (28).

GSH and GSSG determination. [GSH] and [GSSG] were determined as described previously (41) with minor modifications. Briefly, cells were washed twice with HBSS, lifted with a cell scraper (Fisher) into HBSS, and lysed by repeated freeze-thaw cycles. The sample was divided for the determination of two pools, *A* and *B*. *Pool A* consisted of reduced and oxidized GSH, whereas *pool B* included only the oxidized GSH. For *pool A*, the sample was mixed with DTT (50 mM) and Tris (100 mM; pH 8.5). For *pool B*, the sample was mixed with NEM (4 mM), and after 2 min of incubation, Tris (pH 8.5) and DTT (100 mM) were added. In both cases, samples were incubated for 30 min and then 5% SSA was added to precipitate the proteins. The samples were then centrifuged and derivatized with OPA solution (50 mg OPA in a 1:10 methanol-0.4 M potassium borate buffer, pH 9.9) for 5 min at room temperature, and sodium phosphate buffer (pH 7.0) was added. Samples were separated on a reverse-phase column (Atlantis, Waters, Milford, MA) at 30°C coupled to the same type of guard column in a Waters 2695 HPLC system with autosampler system (Waters). Compounds were eluted with 7.5% (vol/vol) methanol in sodium phosphate buffer (10 mM, pH 7.0) and detected with a Hitachi F-1080 fluorescence detector with excitation at 340 nm and emission at 420 nm. Peak areas were integrated with Millennium 3.2 software (Waters). Reduced GSH values were determined by differences between *pools A* and *B*. [GSH] and [GSSG] were expressed per cell, using 6.1 pg DNA/cell (19) and 1.413 pl as cell volume. The reduction potential for the GSSG/2GSH couple was calculated by using the Nernst equation at 37°C and pH 7.2 [half-cell reduction potential (E_{hc}) = -252 mV $-$ (61.5/2)*log([GSH]^2/[GSSG])].

Western blot analysis. IEC-6 cells were seeded at a density of 1.5×10^5 cells in six-well plates on consecutive days. After 2, 3, and 4 days, equal protein concentrations (15 μg) were size separated by 12% SDS-PAGE and transferred to nitrocellulose membranes. Blots were probed with a rabbit polyclonal anti-γ-glutamylcysteine synthetase (γ-GCS) heavy subunit (γ-GCS_H) primary antibody (Neomarkers, Fremont, CA) and horseradish peroxidase-conjugated anti-rabbit IgG (Sigma) as a secondary antibody. Bands were detected with an enhanced chemiluminescence system (ECL, Amersham Biosciences, Piscataway, NJ). Immunoblots were scanned by optical densitometry (GS-710 Calibrated Imaging Densitometer, Bio-Rad, Hercules, CA) to quantify the relative level of protein expression between treatments, using the peak density option in Diversity Database 2.2.0 software (Bio-Rad).

Quantification of ROS and NO. ROS activity was detected by flow cytometric analysis using the fluorescein-labeled dye dichlorodihydrofluorescein diacetate (H_2DCF; Molecular Probes). Cells were treated with 10 μM H_2DCF for 30 min at 37°C, washed with PBS, and dispersed with trypsin, and endogenous peroxides were measured with a MoFlo MLS high-speed flow cytometry instrument (Cytomation). NO production was detected by flow cytometric analysis using the fluorescein-labeled dye 4-amino-5-methylamino-2′,7′-difluorofluorescein (DAF-FM) diacetate (Molecular Probes). Cells were treated with 5 μM H_2DCF for 45 min at 37°C, washed with PBS, and incubated in PBS for 15 min. The cells were then dispersed with trypsin, and NO was measured with the MoFlo MLS high-speed flow cytometry instrument. Data were analyzed with Summit V3.1 software. Ten thousand events were recorded for each analysis. Results were calculated as the mean fluorescence intensity of treated relative to control cells. Results of different experiments were normalized with Immuno-Bright calibration beads (Coulter Source, Marietta, GA).

NAD(P)(H), ATP, and ADP. [NADPH]-to-[$NADP^+$], [NAD^+]-to-[NADH], and [ADP]-to-[ADP] ratios and concentrations were determined according to the method described by Lazzarino et al. (29) with modifications. Briefly, cells were washed with PBS, nitrogen-saturated precipitation solution [acetonitrile-10 mM KH_2PO_4 (3:1) pH 7.4; 4°C] was added, and the cells were collected and centrifuged at 16,000 *g* for 4 min at 4°C. Ice-cold chloroform was added to the supernatant, which was mixed and centrifuged at 16,000 *g* for 4 min at 4°C. Chloroform extraction was repeated twice, keeping the aqueous phase. Samples were filtered and transferred to an autosampler vial or stored at −80°C until HPLC analysis. Separation was performed on a Waters 2695 separations module at 25.5–26°C on a reverse-phase column (Kromasil C18) coupled to a guard column (Waters Symmetry C18), using tetrabutylammonium hydroxide as an ion-pairing reagent. Detection was performed with a Waters 2487 dual absorbance detector at 260 nm [for ATP, ADP, NAD(P)] serially connected to a Hitachi F-1080 fluorescence detector with excitation at 360 nm and emission at 465 nm [for NAD(P)H]. Peak areas were integrated with Millennium 3.2 software. The intracellular E_{hc} values were calculated by the Nernst equation for each NADPH-to-$NADP^+$ ratio [E_{hc} = -321.15 mV $-$ (61.5/2)*log(NADPH/$NADP^+$)] and NADH-to-NAD^+ ratio [E_{hc} = -322.15 mV $-$ (61.5/2)*log(NADH/NAD^+)] at 37°C and pH 7.2.

Statistics. Results are expressed as means ± SE. A minimum of two independent experiments with triplicate samples per time point

were performed per analysis. Statistical analysis was performed with SAS (version 8.02; SAS Institute, Cary, NC). For comparison between days, a general linear model procedure was used [Variable = Day + error (ϵ) and Variable = Day + $(Day)^2$ + ϵ], and a Tukey's *W* procedure was used to separate different populations (SAS 8.02). Comparisons between the different stages were performed with contrasts. Other comparisons were performed with paired Student's *t*-tests (SAS 8.02). Statistical significance was set at $P < 0.05$.

RESULTS

Growth curve and cell cycle analysis. Quaroni et al. (47) reported that IEC-6 cell growth decreased as the culture became denser and eventually ceased by a contact inhibition mechanism. Our observations are consistent with this, showing that cells grew logarithmically from *day 2* to *day 6*, reaching a plateau after *day 7* (Fig. 1*A*). *Day 6* cell numbers were significantly lower compared with *day 8* ($P < 0.05$). Cell cultures became confluent at *day 4*, but the number of cells continued to increase between *days 4* and *8*. After *day 8*, cell number remained constant through *day 12* (Fig. 1*A*). To further characterize the growth of IEC-6 cells, cell cycle analysis was performed by flow cytometry. The percentage of cells in G_0/G_1 cell cycle phase increased significantly for *days 9–12* compared with the earlier days (*days 1–8*, $P < 0.01$; Fig. 1*B*), showing a distinct decrease in cell proliferation after *day 8*.

From these data, three distinct stages of cell growth were defined. *Stage 1* was the period from seeding until the cells became confluent (*day 4*). *Stage 2* was postconfluence from *day 4* until *day 8*, while cells continued proliferating. *Stage 3* was from *day 9* to *day 12*, when cell proliferation decreased by contact inhibition, as evidenced by a significant increase in G_0/G_1 cells.

Intracellular [GSH] and [GSSG] and calculation of redox state of the GSH/GSSG couple. [GSH] increased from *day 1* to *day 3* and then successively decreased until *day 14*. [GSH] on *day 3* were significantly higher and [GSH] on *days 9–14* were significantly lower than the others (Fig. 2*A*). [GSSG] decreased from *day 1* to *day 3* and then increased again from *day 11* to *day 14*. [GSSG] on *days 1*, *2*, *13*, and *14* were significantly higher compared with the other days. From *day 1* to *day 3*, the increase in [GSH] was accompanied by a decrease in GSSG, but the changes in [GSSG] were not of sufficient magnitude to account for the total changes in GSH. A decrease in GSH and the opposite increase in GSSG were also observed during the last 3 days (Fig. 2*A*). The GSSG/2GSH couple became more reduced (−35 mV) from *day 1* to *day 3*, when cells were actively proliferating, and then became more oxidized (+45 mV) toward the end of the study period (Fig. 2*B*). The GSSG/2GSH couple was more oxidized after *day 9* compared with the previous days ($P < 0.01$). The range of reduction potential of the GSSG/2GSH couple varied from -171.6 ± 8.6 mV, when cell growth was arrested by contact inhibition, to -216.8 ± 2.8 mV, when they were actively proliferating on *day 3*, just before confluence. To determine the extent to which observed changes in [GSH] resulted from an increase in de novo synthesis, expression of the catalytic subunit of γ-GCS (γ-GCS_H), the enzyme involved in the rate-limiting step of GSH synthesis (20), was measured. Changes in the amount of γ-GCS_H preceded changes in the synthesis of GSH (Fig. 3). Expression of γ-GCS_H was significantly higher on *day 2*, when GSH concentrations were increasing, lower on *day 3*, when GSH values peaked, and significantly lower on *day 4*, when [GSH] started to decrease (Fig. 3).

Intracellular ROS. To examine the role of ROS during cell growth, ROS production was measured by flow cytometric analysis using H_2DCF, a dye sensitive for several ROS species but not for NO. After an early maximum at *day 1*, ROS production decreased, reaching a minimum on *days 4* and *5*, corresponding with confluence (Fig. 4). Values on *day 1* were

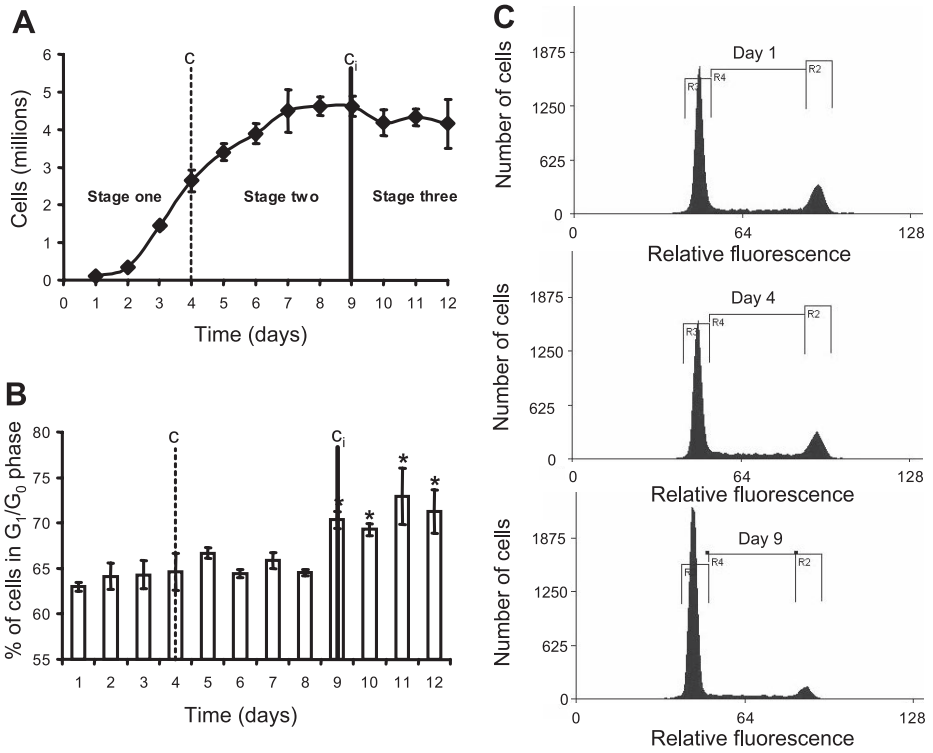

Fig. 1. *A*: growth curve of IEC-6 intestinal epithelial cells. Cells were cultured for the periods indicated, harvested, stained with Trypan blue, and counted with a hemocytometer. *B*: cell cycle analysis of intestinal epithelial cells over time. Cells were cultured for the periods indicated, harvested, stained with propidium iodide, and analyzed by flow cytometry. The percentage of cells in a nonproliferative state (G_1/G_0) after *day 9* was significantly greater than on the preceding days (*$P < 0.01$). C, confluent cells; C_i, contact-inhibited cells. *C*: example of differential cell cycle distribution among *days 1*, *4*, and *9* (R3 = G_1/G_0; R4 = S phase; R2 = G_2/M). The data represent means ± SE for 3 independent experiments in which each time point was measured in triplicate.

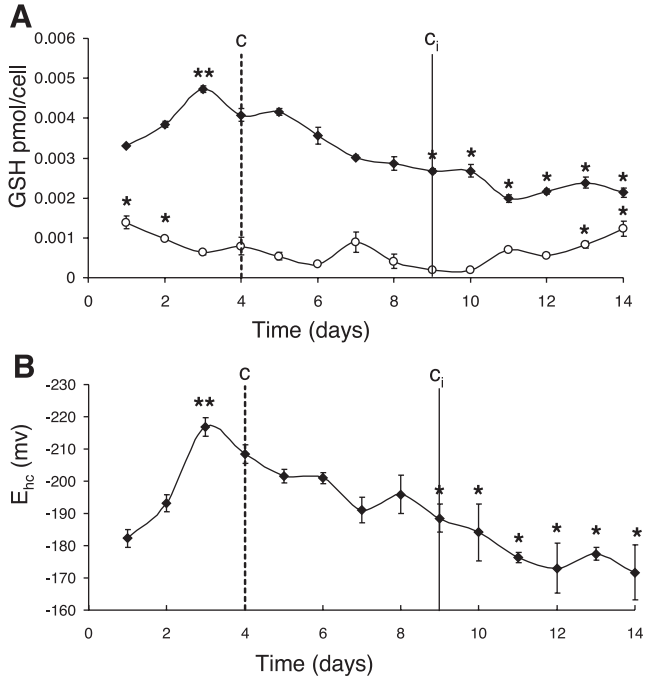

Fig. 2. *A*: intracellular GSH ([GSH]) and GSSG ([GSSG]) concentrations per cell over time. [GSH] and [GSSG] were determined by HPLC as outlined in MATERIALS AND METHODS. [GSH] (♦) increased from *day 1* to *day 3* and then successively decreased toward *day 14*. *Day 3* values were greater (**$P < 0.01$) and values on *days 9–14* were lower than the other days (*$P < 0.01$). [GSSG] (○) decreased from *day 1* to *day 3* and then increased again from *day 11* to *day 14*. GSSG values on *days 1*, *2*, *13*, and *14* were significantly greater than the other days except for *day 7* (*$P < 0.05$). *B*: cellular half-cell reduction potential (E_{hc}) of the GSSG/2GSH couple calculated with the Nernst equation and [GSH] and [GSSG]. The couple became reduced from *day 1* to *day 3* (−35 mV) and then started to become more oxidized. The couple was significantly more reduced on *day 3* (**$P < 0.01$) and more oxidized after *day 9*, when proliferation decreased because of contact inhibition, compared with other days (*$P < 0.01$). The data represent means ± SE for 3 independent experiments in which each time point was measured in triplicate.

significantly greater compared with the rest of the days. After *day 5*, ROS production began to increase, but the values were still lower compared with the values on *days 1–3*. ROS production during *days 1–3* was significantly greater than that on the rest of the days ($P < 0.01$). Values from *day 9* to *day 12*, when cell proliferation decreased, were greater compared with ROS production on *days 5–8* ($P < 0.01$; Fig. 4).

NO production over time. Cellular NO production followed at the beginning (*days 1–4*) a pattern similar to ROS production, starting with a maximum value on *day 1* and then decreased concentrations until *day 3* (Fig. 5). Values on *days 1–3* were significantly greater compared with the rest of the days. At *day 4*, when the cells were reaching confluence, relative NO concentrations decreased drastically. Then NO concentrations continued to decrease until a minimum was reached after *day 6*, with concentrations remaining low and constant until *day 12*. Values from *days 5–12* were similar.

Effects of proliferation and contact inhibition on NADPH, $NADP^+$, NADH, NAD^+, ATP, and ADP. The [NADPH]-to-[$NADP^+$] ratio decreased from *day 2* until *day 4* and then remained constant for the remainder of the growth study (Fig. 6*A*). The ratios on *days 2* and *3* were significantly greater than all the other values ($P < 0.01$). Ratios from *day 4* to *day 12* were similar. The $NADPH^+$/NADPH couple was significantly more reduced at the beginning of the culture (−340.1 ± 1.7 mV; *day 2*) and then decreased until it reached approximately −300 mV at confluence (−305.9 ± 2.6 mV; *day 4*) and did not change significantly after this point. The lowest value was reached on *day 12* (−289.9 ± 1.0 mV). The [NAD^+]-to-[NADH] ratio varied differently, increasing from the beginning of the culture and reaching a maximum after confluence. This ratio was significantly greater on *days 4*, *6*, and *8* compared with the other days ($P < 0.01$). Coincident with the decrease in proliferation after *day 8*, the [NAD^+]-to-[NADH] ratio decreased after *day 8* and toward the end of the growth study (Fig. 6*B*). This couple became oxidized from *day 2* (−302.2 ± 3.2 mV) until *day 6* (−281.8 ± 1.9 mV) and then became reduced again after *day 8*. By *day 12*, the reduction potential of the NAD^+/NADH couple was −309.1 ± 4.4 mV. The NAD^+/NADH couple was significantly more oxidized on *days 4*, *6*, and *8* compared with the rest of the days. The [ATP]-to-[ADP] ratio remained constant throughout the experiment, except at *day 12*, when it increased significantly (Fig. 6*C*).

DISCUSSION

These data indicate that the redox state of distinct couples varies differentially during normal proliferation and contact inhibition, making it difficult to define the intracellular redox status that accompanies these processes by considering only one redox species. To our knowledge, these data are the first to examine the state of multiple redox couples over the course of a temporal growth study with nontransformed epithelial cells. Differential variation in the redox state of various couples may enable multiple protein modifications at different stages, thereby increasing options for redox regulation of cellular processes.

We observed an increase in GSH concentrations at the beginning of the logarithmic growth phase and a subsequent decrease simultaneous with a decrease in proliferation due to contact inhibition. Consistent with previous studies, the data confirm that [GSH] are greater during the exponential growth phase and then decrease as cells become confluent and begin to differentiate (4, 42, 51). The +45-mV oxidation of the E_{hc} of

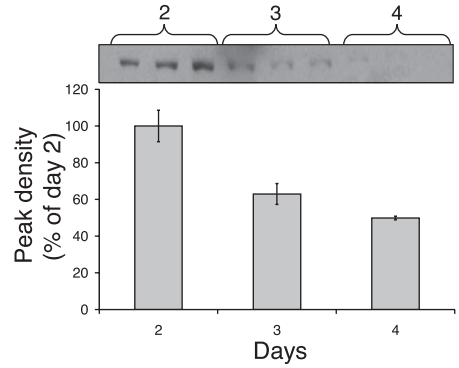

Fig. 3. *Top*: Western blot analysis of γ-glutamylcysteine synthetase heavy subunit (γ-GCS_H) over time. Equal protein concentrations (15 μg) were size separated using 12% SDS-PAGE, transferred to nitrocellulose membranes, and probed for γ-GCS_H as described in MATERIALS AND METHODS. *Bottom*: quantification of the gel bands measuring the peak density. *Day 2* values were significantly greater than those on *days 3* and *4* ($P < 0.01$). The data represent means ± SE for 2 independent experiments in which each time point was measured in triplicate.

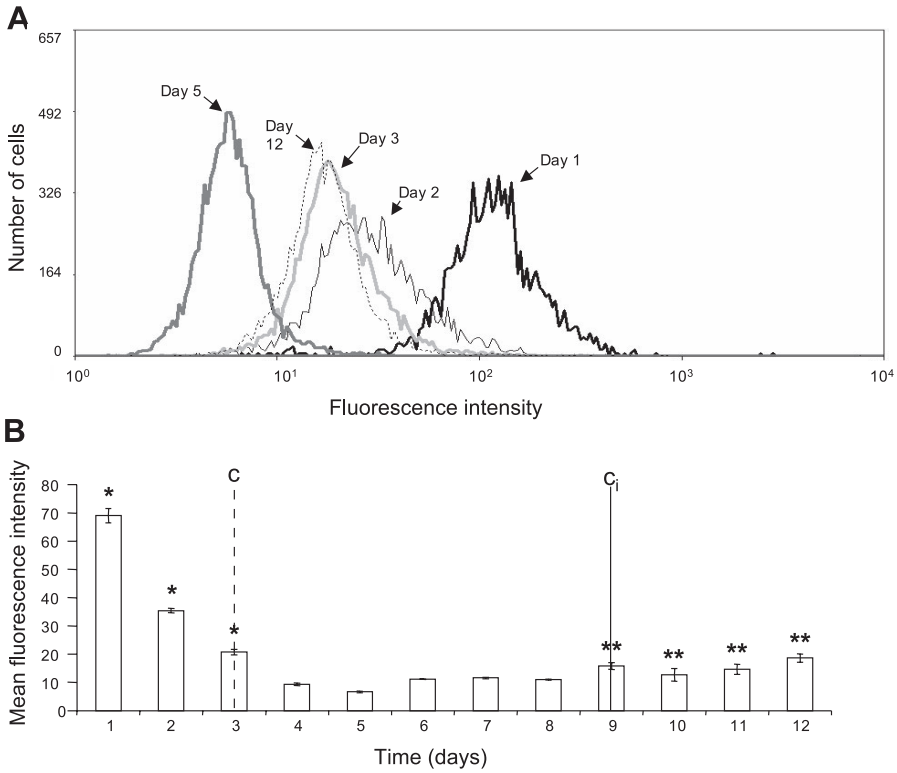

Fig. 4. Cellular reactive oxygen species (ROS) production over time. *A*: changes in the relative fluorescence distribution on different days. *B*: summary of the complete data. Data represent means of the population means ± SE. ROS production reached a maximum at *day 1* and then diminished until *day 5*. After *day 5*, ROS production started to increase slowly until *day 12*. ROS production during *days 1–3* was significantly greater than on the rest of the days (*$P < 0.01$). Values from *day 9* to *day 12* were greater than values from *day 5* to *day 8* (**$P < 0.01$). The data represent the population means ± SE for 3 independent experiments in which each time point was measured in triplicate samples.

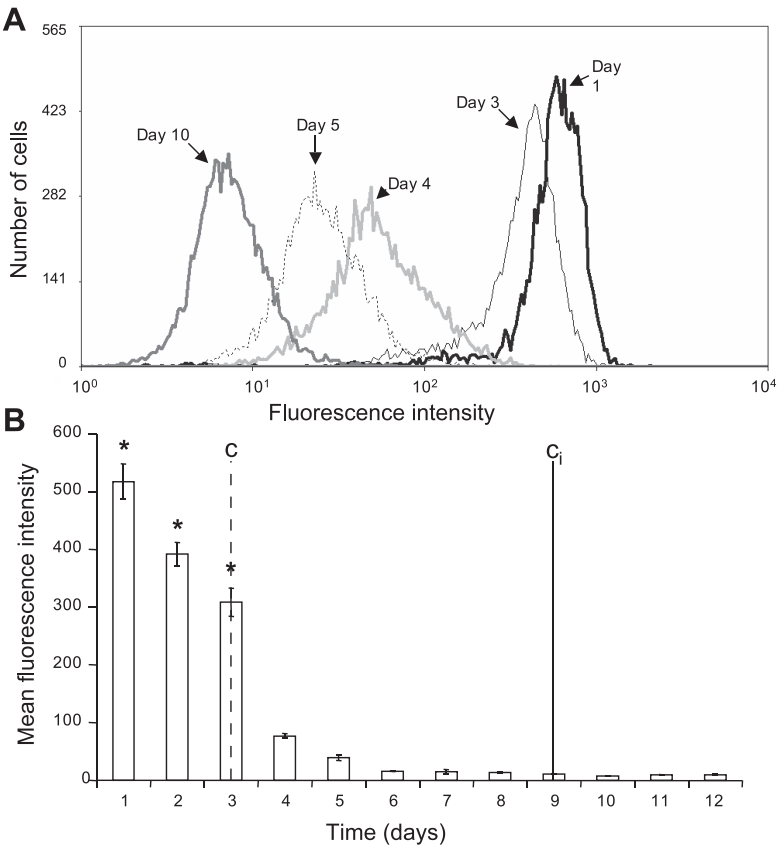

Fig. 5. Cellular nitric oxide (NO) production over time. Cells were cultured for the periods indicated, harvested, stained with 4-amino-5-methylamino-2′,7′-difluorofluorescein diacetate, and analyzed using flow cytometry. *A*: representative flow cytometric data showing differential fluorescence distribution for different days. *B*: summary of the data. Values after *day 5* were similar across days. Values from *day 1* to *day 3* were greater than values on the other days (*$P < 0.01$). The data represent the population means ± SE for 3 independent experiments in which each time point was measured in triplicate samples.

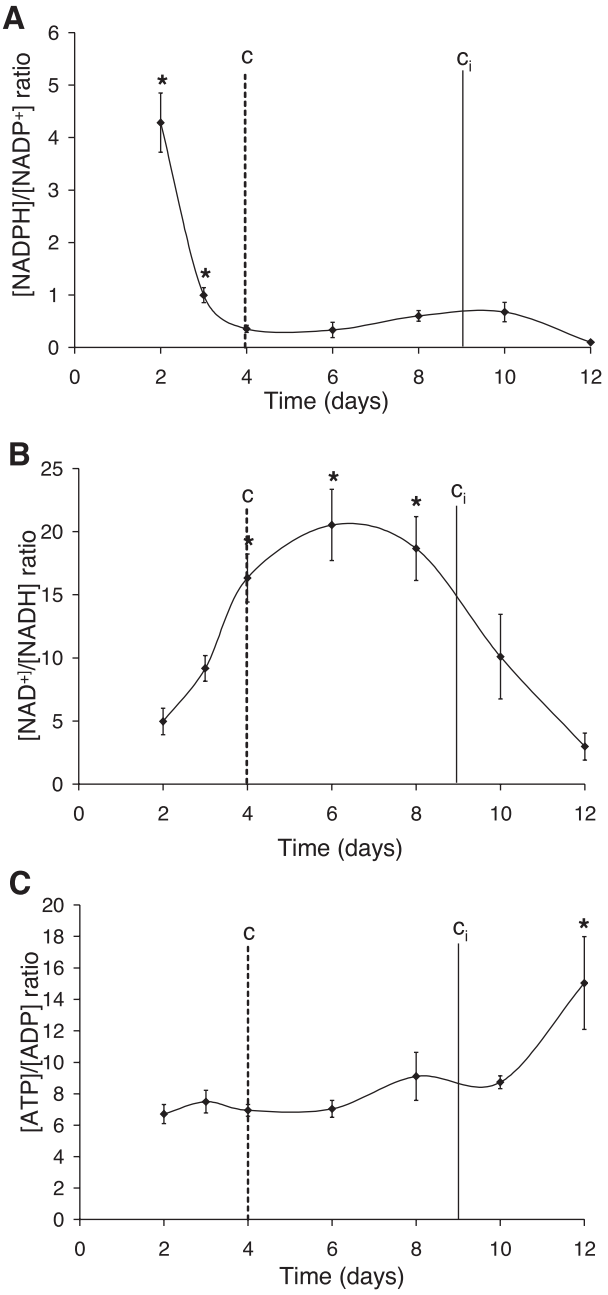

Fig. 6. *A*: NADPH concentration ([NADPH])-to-NADP$^+$ concentration ([NADP$^+$]) ratios over time. The ratio decreased from *day 2* to *day 4* and then remained constant. Ratios on *days 2* and *3* were greater than ratios on the other days (*$P < 0.01$). *B*: NAD$^+$ concentration ([NAD$^+$])-to-NADH concentration ([NADH]) ratios over time. The ratio increased from *day 2* to *day 6* and then decreased after *day 8*. *Days 4*, *6*, and *8* ratios were greater than ratios on the other days (*$P < 0.01$) *C*: ATP concentration ([ATP])-to-ADP concentration ([ADP]) ratios over time. The ratio remained unchanged from *day 2* to *day 10* and then increased on *day 12* (*$P < 0.05$). [NADPH]-to-[NADP$^+$], [NAD$^+$]-to-[NADH], and [ATP]-to-[ADP] ratios were determined using HPLC as outlined in MATERIALS AND METHODS. The data represent means ± SE for 2 independent experiments in which each time point was measured in triplicate.

the GSSG/2GSH couple observed between cells actively proliferating on *day 3* and contact-inhibited cells at *day 12* is similar to published data (5, 22, 42). A change of this magnitude in the redox state of GSH is sufficient to regulate the activity of proteins with redox-sensitive thiols, assuming that sufficient glutaredoxin activity is present to mediate such effects (23, 37, 50). The present data indicate that changes in the GSH pool may be generated in part by shuttling GSH equivalents to and from the GSSG pool. Specifically, [GSSG] and [GSH] fluctuated in opposite directions at the beginning and end of the study. However, the changes in [GSSG] were not of a sufficient magnitude to explain the observed changes in GSH alone. Temporal changes were also observed in expression of γ-GCS$_H$ protein, which is the catalytic subunit of γ-GCS, the rate-limiting enzyme in the de novo synthesis of GSH (20). Together these data indicate that both major pathways in GSH synthesis, de novo production and regeneration of GSH from GSSG, underlie [GSH] changes during cell proliferation. The decrease in γ-GCS$_H$ expression coincided with a decrease in ROS concentrations and an increase in [GSH] during the same period. This is consistent with previous observations that γ-GCS$_H$ synthesis is induced by an increase in ROS (52) and a decrease in GSH (8).

The present study indicates a role for ROS in both proliferation and contact inhibition. These data are consistent with an oxidative event being necessary to initiate proliferation (38, 43) and with previous observations that ROS production is greater in sparse than in confluent cells (45). As suggested by Schafer and Buettner (50), an oxidative stimulus similar to that observed in this study may be responsible for the subsequent increase in [GSH]. This effect may be mediated, at least in part, by activation of γ-GCS transcription through a 5′ antioxidant response element (40). To the contrary, the decrease in proliferation due to contact inhibition was also accompanied by an increase in ROS concentrations, denoting a potential dual effect for ROS in cell proliferation as well as in contact inhibition. The extent of the oxidative stimulus may be responsible for this differential role (15, 50).

NO-mediated signaling is involved in cell proliferation, growth inhibition, and apoptosis (14, 16, 39). In this study, relative [NO] were high at the beginning of the culture period, decreased when the cells reached confluence, and then remained constant, suggesting a role of NO in cell proliferation. Relative [NO] were similar between confluent but proliferating cells compared with contact-inhibited cells, indicating that in contrast to ROS, NO is apparently not involved in signaling related to growth arrest. This observation seems to contradict other findings that NO is associated with the cessation of cell proliferation (16, 57). NO is involved in the regulation of GSH

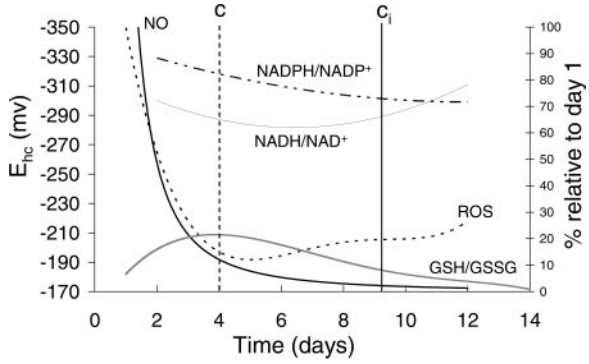

Fig. 7. Summary of the data. Exponential or polynomial curves were used to fit the data. GSSG/2GSH and NAD(P)$^+$/NAD(P)H data are expressed as E_{hc}. ROS and NO data are expressed as % of *day 1* value.

(27) and superoxide concentrations (44). Moreover, high ROS concentrations are responsible for modulating NO bioactivity during cell proliferation (3). Although we observed a temporal relationship among ROS, NO, and GSH, additional studies are needed to determine the extent of cross-regulation among these redox molecules in the context of cell growth regulation.

[NAD(P)H]-to-[NAD(P)$^+$] ratios were high in proliferating cells and low in G_1-arrested cells (36). In agreement, in the present study, the [NADPH]-to-[NADP$^+$] ratio was greatest at the beginning of the culture and then decreased, reaching a minimum at confluence and remaining low through contact inhibition. The decrease in *stage 1* may reflect a flux of electrons from NAD(P)H to GSSG to generate more GSH or the use of NADPH electrons for biosynthetic pathways as well as for ROS and NO production. The NAD$^+$/NADH couple became more oxidized during *stage 1* but was reduced during *stage 3*, when cell proliferation decreased by contact inhibition, contradicting previous observations of an oxidation of NADH during contact inhibition in fibroblasts (7). These couples are capable of acting as sensors of the redox or energetic state of the cell and thereby directly regulate cellular processes (32, 49, 58). The observed changes in the [NADPH]-to-[NADP$^+$] ratio (from 4.3 $\pm$ 0.56 to 0.1 $\pm$ 0.007) and in the [NAD$^+$]-to-[NADH] ratio (from 2.98 $\pm$ 1.07 to 20.5 $\pm$ 2.82) are similar to changes shown to affect the binding properties of transcription factors that regulate expression of the light-dark cycle proteins (49) and may thus be involved in the regulation of cell proliferation and contact inhibition. Interestingly, when cells were contact inhibited, the NAD$^+$/NADH couple was more reduced, the GSSG/2GSH couple was more oxidized, and the [ATP]-to-[ADP] ratio reached its highest value, consistent with the mechanism proposed by Jones (23), in which GSH redox state is controlled by metabolism. In this mechanism, electrons derived from GSH are used to reduce NAD$^+$ to NADH. This creates an electron flux from NADPH to NADH and eventually to the mitochondrial electron transport chain, generating more ATP in cases when the NAD$^+$/NADH couple is oxidized, such as nutrient deprivation.

As summarized in Fig. 7, changes in the redox state of distinct couples are associated with the processes of cell proliferation and growth arrest by contact inhibition. However, the direction of these changes varied among the different couples, indicating that it is not possible to describe the redox state of the cell by examining just one couple. It is more precise to consider changes in the redox state of a specific couple or changes in the concentration of a redox-active species associated with a particular cellular process. In other words, it is not possible to state that the cell is more reduced (or oxidized) when it is actively dividing, but it is possible to indicate that the GSH couple is more reduced in proliferating relative to contact-inhibited cells. Schafer and Buettner (50) defined the redox environment as "the summation of the products of the reduction potential and the reducing capacity of the linked couples present in an organelle, cell or tissue." They pointed out that because the GSSG/2GSH couple provides a relatively large pool of reducing equivalents, its reduction potential effectively determines the intracellular redox environment and correlates with biological stages (proliferation, confluence, differentiation, apoptosis, and necrosis). Although our data generally agree, reliance on this definition alone may overlook an opposite change in another couple present in lower concentrations that may be critical for a particular regulatory mechanism. For example, the present data demonstrate that in *stage 1* of culture, the GSSG/2GSH couple became more reduced while the NAD(P)$^+$/NAD(P)H couples became more oxidized. Furthermore, organelles such as mitochondria, nuclei, and endoplasmic reticulum have differential pools of redox-active species compared with the cytoplasm (6, 56). These independent pools add spatial complexity to the system, providing cells additional regulatory options, perhaps according to organelle-specific processes. In addition to spatial separation, different couples may exhibit dependent or independent changes in redox status, depending on whether they are linked enzymatically.

The idea that multiple independent thiol-redox circuits coexist in the cell has been discussed previously (24). During cell proliferation, the redox states of the GSSG/2GSH, thioredoxin, and cystine/cysteine couples fluctuate independently (24, 42), generating different nodes where proteins can be modified (glutathionylated, *S*-cysteinylated) and functionally altered. The present data extend this idea to nonthiol redox couples and redox species, showing that NAD(P)$^+$/NAD(P)H, ROS, and NO also fluctuate in association with the state of cell growth. Each of these molecules has been shown to react with different proteins and to regulate their activity (13, 17, 49, 55). Each distinct redox species may represent a unique redox or metabolic sensor (not necessarily independent of one another) that controls the activity of separate regulatory proteins by a redox or allosteric mechanism, with the summation of events influencing cell fate decisions. Development of appropriately scaled tools enabling real-time measurements in living cells will be needed to fully define the molecular basis of regulatory mechanisms controlled by local redox potential.

ACKNOWLEDGMENTS

We thank Barbara Pilas and Ben Montez at the Flow Cytometry Facility of the University of Illinois at Urbana-Champaign Biotechnology Center, Mark Kuhlenschmidt (Dept. of Veterinary Pathobiology) for use of the Coulter counter, and Giuseppe Lazzarino for sharing HPLC technical expertise. We thank John Conour and Tarannum Khan for review of the manuscript and Juan Marini for statistical consultation.

Kajorn Kitiphongspattana is currently a Postdoctoral Scholar in the Department of Medicine at the University of Chicago.

Present address of K. Ishii-Schrade: Graduate School of Pharmaceutical Sciences, University of Tokyo, Tokyo, Japan.

GRANTS

This work was supported in part by National Institutes of Health (NIH) Grant R01-DK-061568 (to H. R. Gaskins), by NIH Ruth Kirschstein Institutional National Research Service Award 5T32-DK-59802 (Div. of Nutritional Sciences, University of Illinois at Urbana-Champaign), and by a University of Illinois Predoctoral Fellowship (to M. S. Attene-Ramos).

REFERENCES

1. **Abate C, Patel L, Rauscher FJ 3rd, and Curran T.** Redox regulation of fos and jun DNA-binding activity in vitro. *Science* 249: 1157–1161, 1990.
2. **Albina JE and Henry WL Jr.** Suppression of lymphocyte proliferation through the nitric oxide synthesizing pathway. *J Surg Res* 50: 403–409, 1991.
3. **Arnal JF, Tack I, Besombes JP, Pipy B, and Negre-Salvayre A.** Nitric oxide and superoxide anion production during endothelial cell proliferation. *Am J Physiol Cell Physiol* 271: C1521–C1526, 1996.
4. **Atzori L, Dypbukt JM, Sundqvist K, Cotgreave I, Edman CC, Moldeus P, and Grafstrom RC.** Growth-associated modifications of low-molecular-weight thiols and protein sulfhydryls in human bronchial fibroblasts. *J Cell Physiol* 143: 165–171, 1990.

5. **Aw TY.** Cellular redox: a modulator of intestinal epithelial cell proliferation. *News Physiol Sci* 18: 201–204, 2003.
6. **Bellomo G, Vairetti M, Stivala L, Mirabelli F, Richelmi P, and Orrenius S.** Demonstration of nuclear compartmentalization of glutathione in hepatocytes. *Proc Natl Acad Sci USA* 89: 4412–4416, 1992.
7. **Bereiter-Hahn J, Munnich A, and Woiteneck P.** Dependence of energy metabolism on the density of cells in culture. *Cell Struct Funct* 23: 85–93, 1998.
8. **Cai J, Huang ZZ, and Lu SC.** Differential regulation of γ-glutamylcysteine synthetase heavy and light subunit gene expression. *Biochem J* 326: 167–172, 1997.
9. **Cerutti PA.** Prooxidant states and tumor promotion. *Science* 227: 375–381, 1985.
10. **Chen Q and Ames BN.** Senescence-like growth arrest induced by hydrogen peroxide in human diploid fibroblast F65 cells. *Proc Natl Acad Sci USA* 91: 4130–4134, 1994.
11. **Conour JE, Graham WV, and Gaskins HR.** A combined in vitro/bioinformatic investigation of redox regulatory mechanisms governing cell cycle progression. *Physiol Genomics* 18: 196–205, 2004.
12. **Deplancke B and Gaskins HR.** Redox control of the transsulfuration and glutathione biosynthesis pathways. *Curr Opin Clin Nutr Metab Care* 5: 85–92, 2002.
13. **Droge W.** Free radicals in the physiological control of cell function. *Physiol Rev* 82: 47–95, 2002.
14. **Du M, Islam MM, Lin L, Ohmura Y, Moriyama Y, and Fujimura S.** Promotion of proliferation of murine BALB/C3T3 fibroblasts mediated by nitric oxide at lower concentrations. *Biochem Mol Biol Int* 41: 625–631, 1997.
15. **Dypbukt JM, Ankarcrona M, Burkitt M, Sjoholm A, Strom K, Orrenius S, and Nicotera P.** Different prooxidant levels stimulate growth, trigger apoptosis, or produce necrosis of insulin-secreting RINm5F cells. The role of intracellular polyamines. *J Biol Chem* 269: 30553–30560, 1994.
16. **Garg UC and Hassid A.** Inhibition of rat mesangial cell mitogenesis by nitric oxide-generating vasodilators. *Am J Physiol Renal Fluid Electrolyte Physiol* 257: F60–F66, 1989.
17. **Giustarini D, Rossi R, Milzani A, Colombo R, and Dalle-Donne I.** *S*-glutathionylation: from redox regulation of protein functions to human diseases. *J Cell Mol Med* 8: 201–212, 2004.
18. **Gotoh Y, Noda T, Iwakiri R, Fujimoto K, Rhoads CA, and Aw TY.** Lipid peroxide-induced redox imbalance differentially mediates CaCo-2 cell proliferation and growth arrest. *Cell Prolif* 35: 221–235, 2002.
19. **Gregory TR.** Animal Genome Size Database. http://www.genomesize.com, 2005.
20. **Griffith OW and Mulcahy RT.** The enzymes of glutathione synthesis: γ-glutamylcysteine synthetase. *Adv Enzymol Relat Areas Mol Biol* 73: 209–267, 1999.
21. **Hentze MW, Rouault TA, Harford JB, and Klausner RD.** Oxidation-reduction and the molecular mechanism of a regulatory RNA-protein interaction. *Science* 244: 357–359, 1989.
22. **Hutter DE, Till BG, and Greene JJ.** Redox state changes in density-dependent regulation of proliferation. *Exp Cell Res* 232: 435–438, 1997.
23. **Jones DP.** Redox potential of GSH/GSSG couple: assay and biological significance. *Methods Enzymol* 348: 93–112, 2002.
24. **Jones DP, Go YM, Anderson CL, Ziegler TR, Kinkade JM Jr, and Kirlin WG.** Cysteine/cystine couple is a newly recognized node in the circuitry for biologic redox signaling and control. *FASEB J* 18: 1246–1248, 2004.
25. **Kirlin WG, Cai J, Thompson SA, Diaz D, Kavanagh TJ, and Jones DP.** Glutathione redox potential in response to differentiation and enzyme inducers. *Free Radic Biol Med* 27: 1208–1218, 1999.
26. **Kokura S, Wolf RE, Yoshikawa T, Granger DN, and Aw TY.** Molecular mechanisms of neutrophil-endothelial cell adhesion induced by redox imbalance. *Circ Res* 84: 516–524, 1999.
27. **Kuo PC, Abe KY, and Schroeder RA.** Interleukin-1-induced nitric oxide production modulates glutathione synthesis in cultured rat hepatocytes. *Am J Physiol Cell Physiol* 271: C851–C862, 1996.
28. **Labarca C and Paigen K.** A simple, rapid, and sensitive DNA assay procedure. *Anal Biochem* 102: 344–352, 1980.
29. **Lazzarino G, Amorini AM, Fazzina G, Vagnozzi R, Signoretti S, Donzelli S, Di Stasio E, Giardina B, and Tavazzi B.** Single-sample preparation for simultaneous cellular redox and energy state determination. *Anal Biochem* 322: 51–59, 2003.
30. **Li CQ, Trudel LJ, and Wogan GN.** Nitric oxide-induced genotoxicity, mitochondrial damage, and apoptosis in human lymphoblastoid cells expressing wild-type and mutant p53. *Proc Natl Acad Sci USA* 99: 10364–10369, 2002.
31. **Li N and Oberley TD.** Modulation of antioxidant enzymes, reactive oxygen species, and glutathione levels in manganese superoxide dismutase-overexpressing NIH/3T3 fibroblasts during the cell cycle. *J Cell Physiol* 177: 148–160, 1998.
32. **Lin SJ and Guarente L.** Nicotinamide adenine dinucleotide, a metabolic regulator of transcription, longevity and disease. *Curr Opin Cell Biol* 15: 241–246, 2003.
33. **Lo YY and Cruz TF.** Involvement of reactive oxygen species in cytokine and growth factor induction of c-fos expression in chondrocytes. *J Biol Chem* 270: 11727–11730, 1995.
34. **Magni G, Amici A, Emanuelli M, Orsomando G, Raffaelli N, and Ruggieri S.** Enzymology of NAD^+ homeostasis in man. *Cell Mol Life Sci* 61: 19–34, 2004.
35. **Makino Y, Yoshikawa N, Okamoto K, Hirota K, Yodoi J, Makino I, and Tanaka H.** Direct association with thioredoxin allows redox regulation of glucocorticoid receptor function. *J Biol Chem* 274: 3182–3188, 1999.
36. **Mallery SR, Laufman HB, Solt CW, and Stephens RE.** Association of cellular thiol redox status with mitogen-induced calcium mobilization and cell cycle progression in human fibroblasts. *J Cell Biochem* 45: 82–92, 1991.
37. **Masuda S, Dong C, Swem D, Setterdahl AT, Knaff DB, and Bauer CE.** Repression of photosynthesis gene expression by formation of a disulfide bond in CrtJ. *Proc Natl Acad Sci USA* 99: 7078–7083, 2002.
38. **Menon SG, Sarsour EH, Spitz DR, Higashikubo R, Sturm M, Zhang H, and Goswami PC.** Redox regulation of the G_1 to S phase transition in the mouse embryo fibroblast cell cycle. *Cancer Res* 63: 2109–2117, 2003.
39. **Morbidelli L, Chang CH, Douglas JG, Granger HJ, Ledda F, and Ziche M.** Nitric oxide mediates mitogenic effect of VEGF on coronary venular endothelium. *Am J Physiol Heart Circ Physiol* 270: H411–H415, 1996.
40. **Mulcahy RT, Wartman MA, Bailey HH, and Gipp JJ.** Constitutive and β-naphthoflavone-induced expression of the human γ-glutamylcysteine synthetase heavy subunit gene is regulated by a distal antioxidant response element/TRE sequence. *J Biol Chem* 272: 7445–7454, 1997.
41. **Neuschwander-Tetri BA and Roll FJ.** Glutathione measurement by high-performance liquid chromatography separation and fluorometric detection of the glutathione-orthophthalaldehyde adduct. *Anal Biochem* 179: 236–241, 1989.
42. **Nkabyo YS, Ziegler TR, Gu LH, Watson WH, and Jones DP.** Glutathione and thioredoxin redox during differentiation in human colon epithelial (Caco-2) cells. *Am J Physiol Gastrointest Liver Physiol* 283: G1352–G1359, 2002.
43. **Oberley LW, Oberley TD, and Buettner GR.** Cell division in normal and transformed cells: the possible role of superoxide and hydrogen peroxide. *Med Hypotheses* 7: 21–42, 1981.
44. **Palacios-Callender M, Quintero M, Hollis VS, Springett RJ, and Moncada S.** Endogenous NO regulates superoxide production at low oxygen concentrations by modifying the redox state of cytochrome *c* oxidase. *Proc Natl Acad Sci USA* 101: 7630–7635, 2004.
45. **Pani G, Colavitti R, Bedogni B, Anzevino R, Borrello S, and Galeotti T.** Determination of intracellular reactive oxygen species as function of cell density. *Methods Enzymol* 352: 91–100, 2002.
46. **Pani G, Colavitti R, Bedogni B, Anzevino R, Borrello S, and Galeotti T.** A redox signaling mechanism for density-dependent inhibition of cell growth. *J Biol Chem* 275: 38891–38899, 2000.
47. **Quaroni A, Wands J, Trelstad RL, and Isselbacher KJ.** Epithelioid cell cultures from rat small intestine. Characterization by morphologic and immunologic criteria. *J Cell Biol* 80: 248–265, 1979.
48. **Rao GN and Berk BC.** Active oxygen species stimulate vascular smooth muscle cell growth and proto-oncogene expression. *Circ Res* 70: 593–599, 1992.
49. **Rutter J, Reick M, Wu LC, and McKnight SL.** Regulation of clock and NPAS2 DNA binding by the redox state of NAD cofactors. *Science* 293: 510–514, 2001.
50. **Schafer FQ and Buettner GR.** Redox environment of the cell as viewed through the redox state of the glutathione disulfide/glutathione couple. *Free Radic Biol Med* 30: 1191–1212, 2001.

51. **Shaw JP and Chou IN.** Elevation of intracellular glutathione content associated with mitogenic stimulation of quiescent fibroblasts. *J Cell Physiol* 129: 193–198, 1986.
52. **Shi MM, Kugelman A, Iwamoto T, Tian L, and Forman HJ.** Quinone-induced oxidative stress elevates glutathione and induces gamma-glutamylcysteine synthetase activity in rat lung epithelial L2 cells. *J Biol Chem* 269: 26512–26517, 1994.
53. **Smith J, Ladi E, Mayer-Proschel M, and Noble M.** Redox state is a central modulator of the balance between self-renewal and differentiation in a dividing glial precursor cell. *Proc Natl Acad Sci USA* 97: 10032–10037, 2000.
54. **Suthanthiran M, Anderson ME, Sharma VK, and Meister A.** Glutathione regulates activation-dependent DNA synthesis in highly purified normal human T lymphocytes stimulated via the CD2 and CD3 antigens. *Proc Natl Acad Sci USA* 87: 3343–3347, 1990.
55. **Thannickal VJ and Fanburg BL.** Reactive oxygen species in cell signaling. *Am J Physiol Lung Cell Mol Physiol* 279: L1005–L1028, 2000.
56. **Wahllander A, Soboll S, Sies H, Linke I, and Muller M.** Hepatic mitochondrial and cytosolic glutathione content and the subcellular distribution of GSH-S-transferases. *FEBS Lett* 97: 138–140, 1979.
57. **Yang W, Ando J, Korenaga R, Toyo-oka T, and Kamiya A.** Exogenous nitric oxide inhibits proliferation of cultured vascular endothelial cells. *Biochem Biophys Res Commun* 203: 1160–1167, 1994.
58. **Zhang Q, Piston DW, and Goodman RH.** Regulation of corepressor function by nuclear NADH. *Science* 295: 1895–1897, 2002.
59. **Ziche M, Morbidelli L, Masini E, Amerini S, Granger HJ, Maggi CA, Geppetti P, and Ledda F.** Nitric oxide mediates angiogenesis in vivo and endothelial cell growth and migration in vitro promoted by substance P. *J Clin Invest* 94: 2036–2044, 1994.